An Improved Target-Field Method for the Design of Uniform Magnetic Field Coils in Miniature Atomic Sensors

JING WANG[1,2], BINQUAN ZHOU[1,2], XU LIU[1,2], WENFENG WU[1,2], LINLIN CHEN[3], BANGCHENG HAN[1,2], (Member, IEEE), AND JIANCHENG FANG[1,2], (Member, IEEE)

[1]School of Instrumentation Science and Opto-Electronics Engineering, Beihang University, Beijing 100191, China
[2]Hangzhou Innovation Institute, Beihang University, Hangzhou 310051, China
[3]Department of Aerospace Science and Technology, Space Engineering University, Beijing 101416, China

Corresponding authors: Binquan Zhou (bqzhou@buaa.edu.cn) and Bangcheng Han (hanbangcheng@buaa.edu.cn)

ABSTRACT An improved target field method is proposed for the cylindrical coil design to meet the constraint of limited coil volume. It realizes the design of uniform magnetic field coil by predetermining the coil configuration and optimizing the coordinate positions of the target field points. Compared with conventional methods, this current density distribution is divided into two symmetric subregions to solve the problem of reserving a gap in the coil center for setting the light-passing holes. Therefore, this method is more applicable in the miniature atomic devices with optical paths. Moreover, the overall coil performance can be significantly improved using the optimized configuration of coil design parameters. The numerical evaluation shows that the coil designed by this method has remarkable advantages over the nested saddle coil, whose uniformity performance can be improved by about one order of magnitude. The measurements show that the relative magnetic field uniformities of the proposed coils reach 4×10^{-4} and 3×10^{-4} along the z-axis in the range of $\pm 0.24\ R$. The measurement results match well with the theoretical simulation.

INDEX TERMS Uniform magnetic field coils, target-field method, current density, miniature atomic sensors.

I. INTRODUCTION

A tri-axial magnetic coil system is a core component widely applied in extensively fields, such as atomic sensors [1] and magnetic positioning systems [2]–[4]. In magnetic positioning systems, a tri-axial transmitting coil system is excited to complete an effective tracking process [5]–[8]. While, atomic sensors use different interactions between light and atoms to detect different physical quantities with ultra-high measurement potential. The most studied atomic sensors are atomic magnetometers [9]–[11] and nuclear spin gyros [12]–[14]. Among atomic sensors, the uniformity of magnetic field coils is the most concerned one. The required tri-axial magnetic field system can easily be constructed by multiplexing the same cylindrical structure, two orthogonal

transverse magnetic field coils and a solenoid coil. One of the most widely used transverse magnetic field coil is the saddle coil with an aspect ratio of 1.75. The direction of the magnetic field generated by the saddle coil is along the radius of one thin cylindrical shell [15]–[18]. Wu *et al.* proposed a nested structure of a pair of saddle coils that reduced the aspect ratio to 1 at the same uniformity level [19]. In recent years, atomic sensors tend to be miniaturized, resulting in strict requirements for the size and the uniformity of the coil system [20]–[22].

To overcome the limitation of the coil structure, we took the lead in improving the target-field method (TFM) to design the cylindrical uniform coil with magnetic field along its axis [23]. The TFM was first proposed by Turner in the 1980s [24], [25], and has become the mainstream method for the design of shim and gradient coils [26]–[30]. Turner's method is a continuous current density method that depends

J. Wang *et al.*: Improved Target-Field Method for the Design of Uniform Magnetic Field Coils in Miniature Atomic Sensors

IEEE *Access*

on the uniqueness of the Fourier-space analytical expression to obtain the solution result [31]. Using the stream function, an approximate shape of the coil is obtained by discretizing the current density [32]. However, the size of the coil can't be specified in advance. Later, Forbes *et al.* modified the TFM and pre-confined the coil structure using periodic functions to constrain the current density distribution in order to ensure that the current density vanishes outside a certain finite area [33]–[35]. However, the introduction of constraints led to an ill-conditioned problem in the integral equation for the current density which should be solved by the minimization technique [36]. Moreover, Xu *et al.* proposed a design of the radio-frequency phased-array coil with a better magnetic field homogeneity, where the current density on the coil surface was divided into several independent subregions [37]. The application of TFM in the design of shim and gradient coils has proved its advantages of strong adaptability and flexible control of coil structures. However, a thorough analysis of TFM in the design of compact uniform coils with high homogeneity has been rarely performed in the literature. This motivated the authors to utilize the TFM to design uniform magnetic field coils.

In this paper, a design method based on TFM is proposed for the design of cylindrical uniform magnetic field coils. In the proposed method, the magnetic field generated by the coil is distributed along a specific diameter of the cylinder. For the purpose of arranging the pumping and detecting optical paths conveniently, the condition of reserved light-passing holes in the coil center is considered. In order to validate this method, several coil winding patterns are constructed. The experimental results are in good agreement with the simulation results. In the specified target sphere region, the absolute magnetic field relative error of both designed coils is better than 0.001. Compared with traditional design methods, the outstanding advantage of our method is that the coil volume can be first determined according to practical requirements, and then winding patterns can be optimized to meet homogeneity requirements. Therefore, this method is applicable for miniature atomic sensors, where the performance is subjected to the homogeneity of coils.

II. THEORY

The uniform magnetic field coil is fixed on a cylindrical surface of radius R and total height $2H$ along the z-axis (Fig.1). Its ends coincide with the two planes given by $z = \pm H$. Suppose that a continuous current density $\mathbf{J}$ (A/m) is distributed on the surface of the coil that generates the desired magnetic field inside a target spherical volume (TSV) with a radius of cr. Before determining the expression of the current density, the coil surface is evenly divided into two equal sections along the height coordinate due to the highly homogeneous magnetic field in the TSV and the possibility of having light-passing holes. Moreover, the current density in each section is symmetrical along the axis $z = 0$.
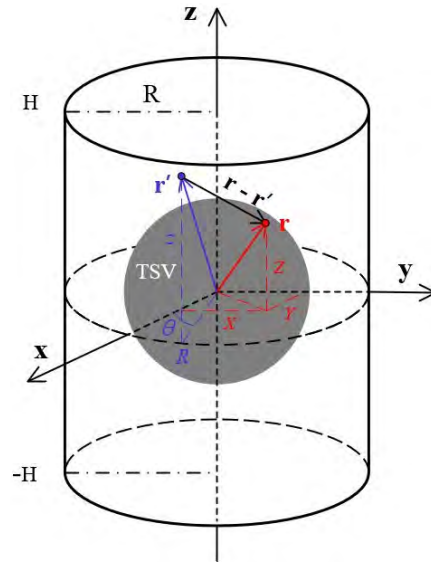
FIGURE 1. A cylindrical coil of radius R and height $2H$ with a target region (TSV) located at the center. A random field point $r(X, Y, Z)$ and a random source point $r'(R, \theta, z)$ are shown.

A. CURRENT DENSITY AND MAGNETIC FIELD RELATIONSHIP

To design such a uniform magnetic field coil, the current density must first satisfy the steady flow condition, as (2.5) in [34]. In this paper, it is expressed as:

$$\nabla \cdot \mathbf{J} = \frac{1}{R}\frac{\partial J_\theta(\theta, z)}{\partial \theta} + \frac{\partial J_z(\theta, z)}{\partial z} = 0. \quad (1)$$

A series of basic trigonometric functions can be selected as the expression of current density in the cylindrical coordinate system [27], [38]. Using the periodicity of the trigonometric functions, the coil current can be set on a cylindrical plane with limited height of $[-H, H]$. At this point, the current density on the coil surface appears as a continuous quantity. In order to generate a uniform magnetic field along the radial direction of a cylindrical coil, $\mathbf{J}$ can be expressed as [34]:

$$\begin{cases} J_{z1}(\theta, z) = -\sum_{n=1}^{N}\sum_{m=1}^{M}\frac{mP_{mn}}{R}\cos(m\theta)\sin(\frac{n\pi(z+H)}{H-Z_0}), \\ J_{\theta 1}(\theta, z) = \sum_{n=1}^{N}\sum_{m=1}^{M}\frac{n\pi P_{mn}}{H-Z_0}\sin(m\theta)\cos(\frac{n\pi(z+H)}{H-Z_0}), \\ \qquad\qquad\qquad\qquad\qquad (-H \leq z \leq -Z_0), \end{cases} \quad (2)$$

$$\begin{cases} J_{z2}(\theta, z) = -\sum_{n=1}^{N}\sum_{m=1}^{M}\frac{mQ_{mn}}{R}\cos(m\theta)\sin(\frac{n\pi(z-H)}{Z_0-H}), \\ J_{\theta 2}(\theta, z) = \sum_{n=1}^{N}\sum_{m=1}^{M}\frac{n\pi Q_{mn}}{Z_0-H}\sin(m\theta)\cos(\frac{n\pi(z-H)}{Z_0-H}), \\ \qquad\qquad\qquad\qquad\qquad (Z_0 \leq z \leq H), \end{cases} \quad (3)$$

where J_{z1}, J_{z2} and $J_{\theta 1}$, $J_{\theta 2}$ denote the components of $\mathbf{J}$ in the z and θ directions, respectively. P_{mn} and Q_{mn} are the

coefficients of the required current density expression. m and n represent the order of Fourier series terms, whose maximum values are up to M and N. Z_0 is the half of the space width reserved in the center region of the coil for light-passing holes. It is noted that within the area given by $|z| > H$ and $|z| < Z_0$, $\mathbf{J} = 0$ holds, which indicates that the current is in a limited area.

Based on the Biot-Savart's law, the magnetic field produced by the current density can be expressed as:

$$\mathbf{B}(\mathbf{r}) = \frac{\mu_0}{2\pi} \int \int_s \frac{\mathbf{J}(\mathbf{r}') \times (\mathbf{r} - \mathbf{r}')}{||\mathbf{r} - \mathbf{r}'||^3} dA', \qquad (4)$$

where dA' is an integral element of the surface area of $\mathbf{J}(\mathbf{r}')$, μ_0 represents the permeability of vacuum, $\mathbf{r}(X, Y, Z)$ and $\mathbf{r}'(R, \theta, z)$ are the position vectors of one field point and one source point on the coil surface, while $(\mathbf{r} - \mathbf{r}')$ is the distance between them.

Converting the current density in the polar coordinate to the Cartesian coordinate, $\mathbf{J}(\mathbf{r}')$ can be represented as:

$$\mathbf{J}(\mathbf{r}') = -[J_{\theta 1}(\theta, z) + J_{\theta 2}(\theta, z)] \sin \theta \mathbf{e}_x + [J_{\theta 1}(\theta, z)$$
$$+ J_{\theta 2}(\theta, z)] \cos \theta \mathbf{e}_y + [J_{z1}(\theta, z) + J_{z2}(\theta, z)] \mathbf{e}_z, \quad (5)$$

where unit vectors $\mathbf{e}_x$, $\mathbf{e}_y$ and $\mathbf{e}_z$ point to the x-axis, y-axis and z-axis, respectively.

Meanwhile, the magnetic field can be expressed in the Cartesian coordinate as:

$$\mathbf{B}(\mathbf{r}) = B_x(X, Y, Z)\mathbf{e}_x + B_y(X, Y, Z)\mathbf{e}_y + B_z(X, Y, Z)\mathbf{e}_z. \tag{6}$$

The three components of the magnetic field $B_x(X, Y, Z)$, $B_y(X, Y, Z)$ and $B_z(X, Y, Z)$ can be obtained by substituting (5) and (6) into (4). Therefore, the result of the magnetic field along the y-axis is:

$$B_y(X, Y, Z) = \frac{\mu_0 R}{2\pi} \int \int [J_z(\theta, z)(R \cos \theta - X)$$
$$- J_\theta(\theta, z) \sin \theta (Z - z)] \times [(R \cos \theta - X)^2$$
$$+ (R \sin \theta - Y)^2 + (z - Z)^2]^{-3/2} dz d\theta, \quad (7)$$

where $J_\theta(\theta, z) = J_{\theta 1}(\theta, z) + J_{\theta 2}(\theta, z)$, $J_z(\theta, z) = J_{z1}(\theta, z) + J_{z2}(\theta, z)$.

Since the expression of $J_{\theta 1}$, $J_{\theta 1}$, J_{z1} and J_{z1} are defined in (2) and (3), and subjecting to certain transformations, the final expression of $B_y(X, Y, Z)$ is:

$$B_y(X, Y, Z) = \sum_{n=1}^{N} \sum_{m=1}^{M} (P_{mn} U_{mn} + Q_{mn} V_{mn}), \qquad (8)$$

where intermediate functions U_{mn} and V_{mn} are defined as:

$$U_{mn} = \frac{\mu_0 R}{2\pi} \int_0^{2\pi} \int_{-H}^{-Z_0} [\frac{n\pi}{H - Z_0} \sin(m\theta) \cos(\frac{n\pi(z + H)}{H - Z_0})$$
$$\times \sin\theta(Z - z) + \frac{m}{R} \cos(m\theta)$$
$$\times \sin(\frac{n\pi(z + H)}{H - Z_0})(R\cos\theta - X)]$$

$$\times [R^2 + z^2 - 2Zz - 2R(X\cos\theta + Y\sin\theta)$$
$$+ X^2 + Y^2 + Z^2]^{-3/2} dz d\theta, \qquad (9)$$

$$V_{mn} = \frac{\mu_0 R}{2\pi} \int_0^{2\pi} \int_H^{Z_0} [\frac{n\pi}{Z_0 - H} \sin(m\theta) \cos(\frac{n\pi(z - H)}{Z_0 - H})$$
$$\sin\theta(Z - z) + \frac{m}{R} \cos(m\theta)$$
$$\times \sin(\frac{n\pi(z - H)}{Z_0 - H})(R\cos\theta - X)]$$
$$\times [R^2 + z^2 - 2Zz - 2R(X\cos\theta + Y\sin\theta)$$
$$+ X^2 + Y^2 + Z^2]^{-3/2} dz d\theta. \qquad (10)$$

The objective is to find a specific solution of this current density to produce the desired uniform magnetic field as a constant B_{target}. Therefore, in the TSV there would be:

$$B_y(X, Y, Z) = B_{\text{target}}. \qquad (11)$$

The substitution of (8) into (11) causes a highly ill-conditioned problem, leading to the dilemma where a unique solution may not be obtained for a given target field B_{target}. This is attributed to Fredholm integral equations of the first kind. To overcome this ill-conditioned problem, a regularization strategy (Tikhonov regularization) and a penalty function are implemented to determine the unknown coefficients in the expression of the current density.

B. SOLUTION METHOD

Firstly, total number Num of position coordinates of several field points are selected in the target region. Thus, the error function, E, representing the sum of the square of the difference between the calculated magnetic field and the desired magnetic field can be written as:

$$E = \sum_{j=1}^{Num} [B_{y,j}(X_j, Y_j, Z_j) - B_{\text{target}}]^2, \qquad (12)$$

where $B_{y,j}(X_j, Y_j, Z_j)$ is the magnetic field component along the $y-$axis of the jth target field point.

Substituting (8) into (12), the error function can be found as:

$$E = \sum_{j=1}^{Num} [\sum_{n=1}^{N} \sum_{m=1}^{M} (P_{mn} U_{mn}(X_j, Y_j, Z_j)$$
$$+ Q_{mn} V_{mn}(X_j, Y_j, Z_j)) - B_{\text{target}}]^2. \qquad (13)$$

In order to avoid the ill-conditioned problem when solving the undetermined coefficients, Tikhonov regularization is implemented [34].

Then a penalty function F (which relates to the undetermined coefficients) combined with a penalty factor λ is introduced to apply a constraint on the error function. Thus, the residual error E' is modified to be:

$$E'(P_{mn}, Q_{mn}) = E(P_{mn}, Q_{mn}) + \lambda F(P_{mn}, Q_{mn}). \qquad (14)$$

J. Wang *et al.*: Improved Target-Field Method for the Design of Uniform Magnetic Field Coils in Miniature Atomic Sensors

IEEE *Access*

Obviously, the minimal value of E' can be obtained by requiring the derivatives to be zero:

$$\begin{cases} \dfrac{\partial E'}{\partial P_{m'n'}} = \dfrac{\partial E}{\partial P_{m'n'}} + \lambda \dfrac{\partial F}{\partial P_{m'n'}} = 0, \\ \dfrac{\partial E'}{\partial Q_{m'n'}} = \dfrac{\partial E}{\partial Q_{m'n'}} + \lambda \dfrac{\partial F}{\partial Q_{m'n'}} = 0. \end{cases} \quad (15)$$

where m' and n' are the index of the independent variable P_{mn} and Q_{mn}, $m' = 1, 2, \cdots, M$, $n' = 1, 2, \cdots, N$.

The solution of (15) is a series of linear equations that can be represented into matrix form as:

$$(\mathbf{A} + \lambda \Gamma^{\mathrm{T}} \Gamma) \mathbf{x} = \mathbf{W}^{\mathrm{T}} B_{\text{target}}, \quad (16)$$

where Γ is known as the regularization matrix derived from the penalty function. $\mathbf{x} = (P_{11}, P_{12}, \cdots, P_{MN}, Q_{11}, Q_{12}, \cdots, Q_{MN})^{\mathrm{T}}$ is a column vector of all undetermined coefficients. $\mathbf{W} = (wu_{11}, wu_{12}, \cdots, wu_{MN}, wv_{11}, wv_{12}, \cdots, wv_{MN})$ is related to the intermediate functions of length $2MN$, where $wu_{mn} = \sum_{j=1}^{Num} U_{mn}(X_j, Y_j, Z_j)$, and $wv_{mn} = \sum_{j=1}^{Num} V_{mn}(X_j, Y_j, Z_j)$. Matrix $\mathbf{A} = \mathbf{W}^{\mathrm{T}} \mathbf{W}$.

Based on the Tikhonov regularization, an explicit solution of undetermined coefficients, denoted by $\hat{\mathbf{x}}$, can be given by:

$$\hat{\mathbf{x}} = (\mathbf{A}^{\mathrm{T}} \mathbf{A} + \lambda \Gamma^{\mathrm{T}} \Gamma)^{-1} \mathbf{A}^{\mathrm{T}} \mathbf{W}^{\mathrm{T}} B_{\text{target}}. \quad (17)$$

C. STREAM FUNCTION AND OPTIMIZATION OF COIL WINDING PATTERNS

In TFM, the stream function is one of the most commonly used means for generating the winding patterns of the coil system [32]. The winding patterns for the designed coils are obtained from the contours of the stream function. Considering the current continuity equation presented in (1), the stream function can be obtained related to the components of the current density as:

$$J_\theta = \frac{\partial \psi}{\partial z} \text{ and } J_z = -\frac{1}{R} \frac{\partial \psi}{\partial \theta}. \quad (18)$$

Therefore, according to the division of the presented current density expression, the corresponding stream function can also be written into two parts as:

$$\begin{cases} \psi_1(\theta, z) = \sum_{n=1}^{N} \sum_{m=1}^{M} P_{mn} \sin(m\theta) \sin(\dfrac{n\pi(z+H)}{H - Z_0}), \\ \qquad\qquad\qquad\qquad\qquad (-H \le z \le -Z_0), \\ \psi_2(\theta, z) = \sum_{n=1}^{N} \sum_{m=1}^{M} Q_{mn} \sin(m\theta) \sin(\dfrac{n\pi(z-H)}{Z_0 - H}), \\ \qquad\qquad\qquad\qquad\qquad (Z_0 \le z \le H). \end{cases} \quad (19)$$

Another key factor is to select an appropriate type of the penalty function F. In this case, the curvature of the stream function serves as the penalty function in order to optimize

FIGURE 2. Total 147 selected target field points (black points) that are evenly distributed on the surface of three spheres (inner, middle, and outer spheres).

the coil winding patterns. The penalty function is:

$$\begin{cases} F_1 = \displaystyle\int\int_{s1} |\overset{2}{\nabla} \psi_1|^2 \mathrm{d}A' \\ \quad = \displaystyle\int_{-H}^{-Z_0} \int_0^{2\pi} (\dfrac{1}{R^2} \dfrac{\partial^2 \psi_1}{\partial \theta^2} + \dfrac{\partial^2 \psi_1}{\partial z^2})^2 R d\theta dz, \\ F_2 = \displaystyle\int\int_{s2} |\overset{2}{\nabla} \psi_2|^2 \mathrm{d}A' \\ \quad = \displaystyle\int_{Z_0}^{H} \int_0^{2\pi} (\dfrac{1}{R^2} \dfrac{\partial^2 \psi_2}{\partial \theta^2} + \dfrac{\partial^2 \psi_2}{\partial z^2})^2 R d\theta dz. \end{cases} \quad (20)$$

Substituting (19) into (20) provides the final expression of the penalty function as:

$$\begin{cases} F_1 = \dfrac{\pi R(H - Z_0)}{2} \displaystyle\sum_{n=1}^{N} \sum_{m=1}^{M} \left[\dfrac{m^2}{R^2} + \dfrac{n^2\pi^2}{(H - Z_0)^2} \right]^2 P_{mn}^2, \\ F_2 = \dfrac{\pi R(H - Z_0)}{2} \displaystyle\sum_{n=1}^{N} \sum_{m=1}^{M} \left[\dfrac{m^2}{R^2} + \dfrac{n^2\pi^2}{(Z_0 - H)^2} \right]^2 Q_{mn}^2. \end{cases} \quad (21)$$

Thus, the regularization matrix in (16) can be expressed as:

$$\Gamma = \begin{bmatrix} \Gamma_{11} & 0 & \cdots & 0 \\ 0 & \Gamma_{12} & \cdots & 0 \\ \vdots & \ddots & \ddots & \vdots \\ 0 & 0 & \cdots & \Gamma_{MN} \\ \Gamma'_{11} & 0 & \cdots & 0 \\ 0 & \Gamma'_{12} & \cdots & 0 \\ \vdots & \ddots & \ddots & \vdots \\ 0 & 0 & \cdots & \Gamma'_{MN} \end{bmatrix}, \quad (22)$$

where $\Gamma_{mn} = \sqrt{\dfrac{\pi R(H - Z_0)}{2}} (\dfrac{m^2}{R^2} + \dfrac{n^2\pi^2}{(H - Z_0)^2})$, and $\Gamma'_{mn} = \sqrt{\dfrac{\pi R(H - Z_0)}{2}} (\dfrac{m^2}{R^2} + \dfrac{n^2\pi^2}{(Z_0 - H)^2})$.

III. DESIGN AND OPTIMIZATION

To demonstrate the effectiveness of this method, several design examples of winding patterns were constructed. All parameters were selected in accordance with the practical constraints. In this section, two types of coils are listed. One coil provides $Z_0 = 0$ with no light-passing holes, while

the second coil provides $Z_0 = 2.5$ mm to retain light-passing holes.

The dimension of each coil is limited on a cylindrical surface with a radius of $R = 20$ mm and a height of up to $2H = 50$ mm, respectively. The radius of the TSV was $cr = 5$ mm (a quarter of the radius length), and the desired magnetic field was non-zero constant. The uniformity of the magnetic field in TSV is closely related to the Fourier series terms. It was observed that satisfactory accuracy could be achieved with $M = N = 4$.

The selection of the coordinate positions of the target field points is vital to maximize the optimization space. After several theoretical verifications, a total number of $Num = 147$ target field points were evenly distributed on the surfaces of three spheres, as shown in Fig.2. In the absence of light-passing holes, the radiuses of the inner, middle, and the outer sphere were 2 mm, 4.7 mm, and 6.6 mm, respectively. Meanwhile, the radiuses of the inner, middle, and the outer sphere were 2.3 mm, 4.6 mm, and 5.8 mm, respectively, with the consideration of light-passing holes.

The penalty factor λ provides constraints for the regularity and the smoothness of the designed coil windings. The larger λ is, the smoother and more symmetrical the current density distribution on the coil surface will be. However, an extremely large value of λ will reduce the magnetic field accuracy in the target area. Therefore, an appropriate selection of the penalty factor is required to maintain a balance between coil array simplicity and magnetic field homogeneity. Hence, λ was selected to be 10^{-11} and 10^{-12} for the considerations of with and without light-passing holes, respectively.

The above-mentioned parameters were used to calculate the values of the stream functions and the corresponding contours for the designed coils. The resultant stream functions and the contours are shown in Fig.3. The stream functions represented by Fig.3 (a) and (c) coincide with the case of $Z_0 = 0$ and $Z_0 = 2.5$ mm, respectively. After the continuous stream functions were discretized, the discrete line patterns in Fig.3 (b) and (d) were obtained as the current routing of the designed coil. It is obvious that a blank position of 5 mm is left in the middle of Fig.3 (d). The two winding patterns derived from their contours are shown in Fig.4.

IV. CONTRAST

The coils designed using the proposed method have the advantage of large uniform region while a limited volume. The performances of the designed coils are evaluated and compared with the commonly used saddle coil structure. It should be noted that the uniformity performance of the nested saddle coil is better than the single saddle coil [19]. Therefore, nested saddle coil is considered here for a comparative simulation. The geometries of the saddle and the nested saddle coil are shown in Fig.5. Moreover, the two designed coils were processed by the double sided Flexible Printed Circuit (FPC) technology in order to experimentally validate the accuracy of the simulation results.
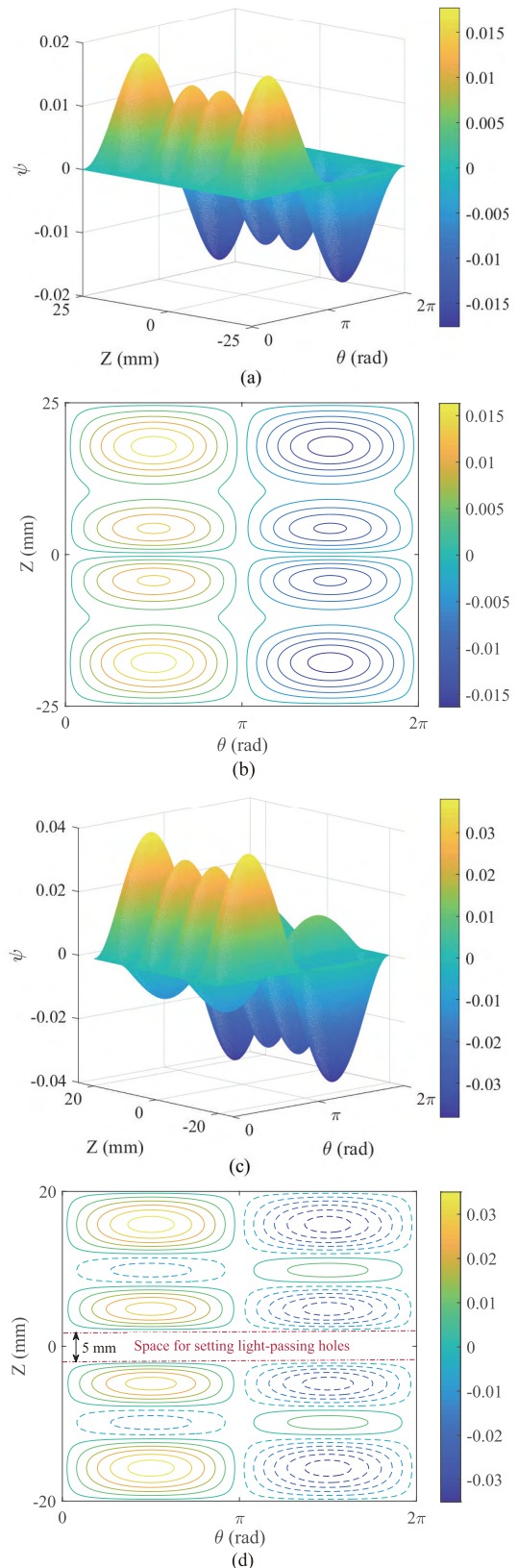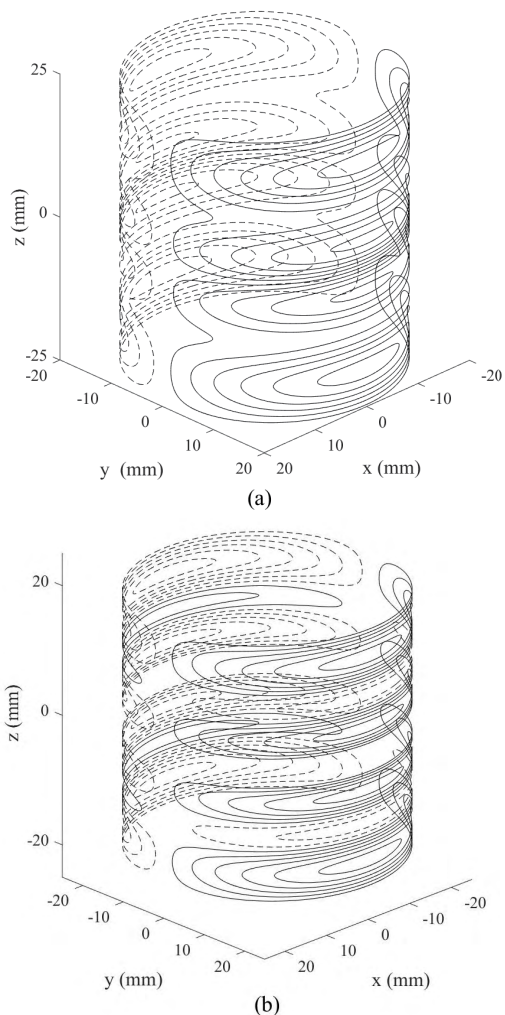

FIGURE 3. Continuous stream functions: (a) $Z_0 = 0$, and (c) $Z_0 = 2.5$ mm. Discretized contour distributions of the stream functions: (b) $Z_0 = 0$, and (d) $Z_0 = 2.5$ mm.

J. Wang *et al.*: Improved Target-Field Method for the Design of Uniform Magnetic Field Coils in Miniature Atomic Sensors

IEEE *Access*

(a)

(b)

FIGURE 4. Winding patterns of the designed coils: (a) $Z_0 = 0$, without light-passing holes; (b) $Z_0 = 2.5$ mm, with light-passing holes. The currents in the solid and the dashed coils run clockwise and counter-clockwise from outside the coil looking in, respectively.
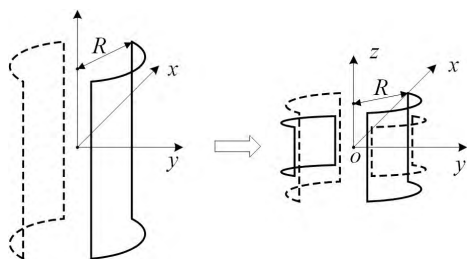
FIGURE 5. The geometries of saddle and nested saddle coils.

A. NUMERICAL ANALYSIS

Here, Biot-Savart's law is applied to compute the resultant magnetic field produced inside the coil. The three types of coils used in this numerical analysis are: two coils designed by this method of $Z_0 = 0$ (aspect ratio of 1.25) and $Z_0 = 2.5$mm (aspect ratio of 1), referred as designed coil 1 and designed coil 2, respectively, and the nested saddle coil (aspect ratio of 1). For a fair comparison, all the simulated coils share the same radius of $R = 20$ mm. Once the coil

TABLE 1. Proportion of the magnetic field relative uniformity in the target region.

Relative uniformity	Designed coil 1	Designed coil 2	Nested saddle coil
$\leq 10^{-5}$	20.57 %	4.38 %	2.94 %
$10^{-5} \sim 10^{-4}$	63.97 %	27.68 %	10.84 %
$10^{-4} \sim 10^{-3}$	15.46 %	67.94 %	39.00 %
$10^{-3} \sim 10^{-2}$	——	——	44.67 %
$> 10^{-2}$	——	——	2.55 %

winding pattern is determined, the magnetic field uniformity of this coil can be reflected regardless of the shape of the target region. Therefore, the target region is selected as a cube with a side length of 10 mm ($R/2$) located in the center of each coil.

The proportion of the magnetic field relative uniformity in the target region is shown in Table 1, and the simulation results of the magnetic field relative error on the three coordinate planes are shown in Fig.6. In the target region, the absolute maximum magnetic field relative errors of the both designed coils are less than 0.001 compared to the error value of 0.012 for the nested saddle coil. The small relative error indicates that the proposed method has a good uniformity performance. Especially, the absolute maximum magnetic field relative error for designed coil 1 is only 4.29×10^{-4}. For designed coil 1 and 2, the volumes of the absolute magnetic field relative errors less than 1×10^{-4} occupy 84.54 % and 32.06 % of the entire target region space, respectively. However, this metric is only 13.79 % for the nested saddle coil. It is obvious that the uniformity performance of the nested saddle coil is barely satisfactory compared with the uniform coils designed by this method.

## B. FABRICATION OF COILS AND MAGNETIC INDUCTION MEASUREMENT

In order to determine the magnetic properties of the fabricated coils and to compare with the numerical analysis results, the magnetic inductions were measured. The designed coil 1, designed coil 2 and nested saddle coil were fabricated by double sided FPC technology with a thickness of only 0.1 mm. Then the coils were glued on the surface of a cylindrical frame with a radius of 63 mm and were each tested separately with a flux-gate magnetometer as shown in Fig.7. Thus, the actual radius of each test coil is 63.1 mm (taking thickness of the test coil into account) compared to the design size. The overall structure of the coil winding enlarges equally with this proportion. The flux-gate magnetometer MAG-03 produced by Bartington Instruments was used for testing. MAG-03 has a measuring range of $[-100\,\mu\text{T}, 100\,\mu\text{T}]$ and a low noise below 6 pTrms/Hz$^{1/2}$ at 1 Hz. In order to avoid the interference of the environmental magnetic field fluctuations and to achieve a precision measurement, the AC modulation and demodulation method [19] was adopted. Two kinds of experiments were conducted. The first experiment was to measure the magnetic field produced by the coil with an unchanged amplitude of the modulated current at various
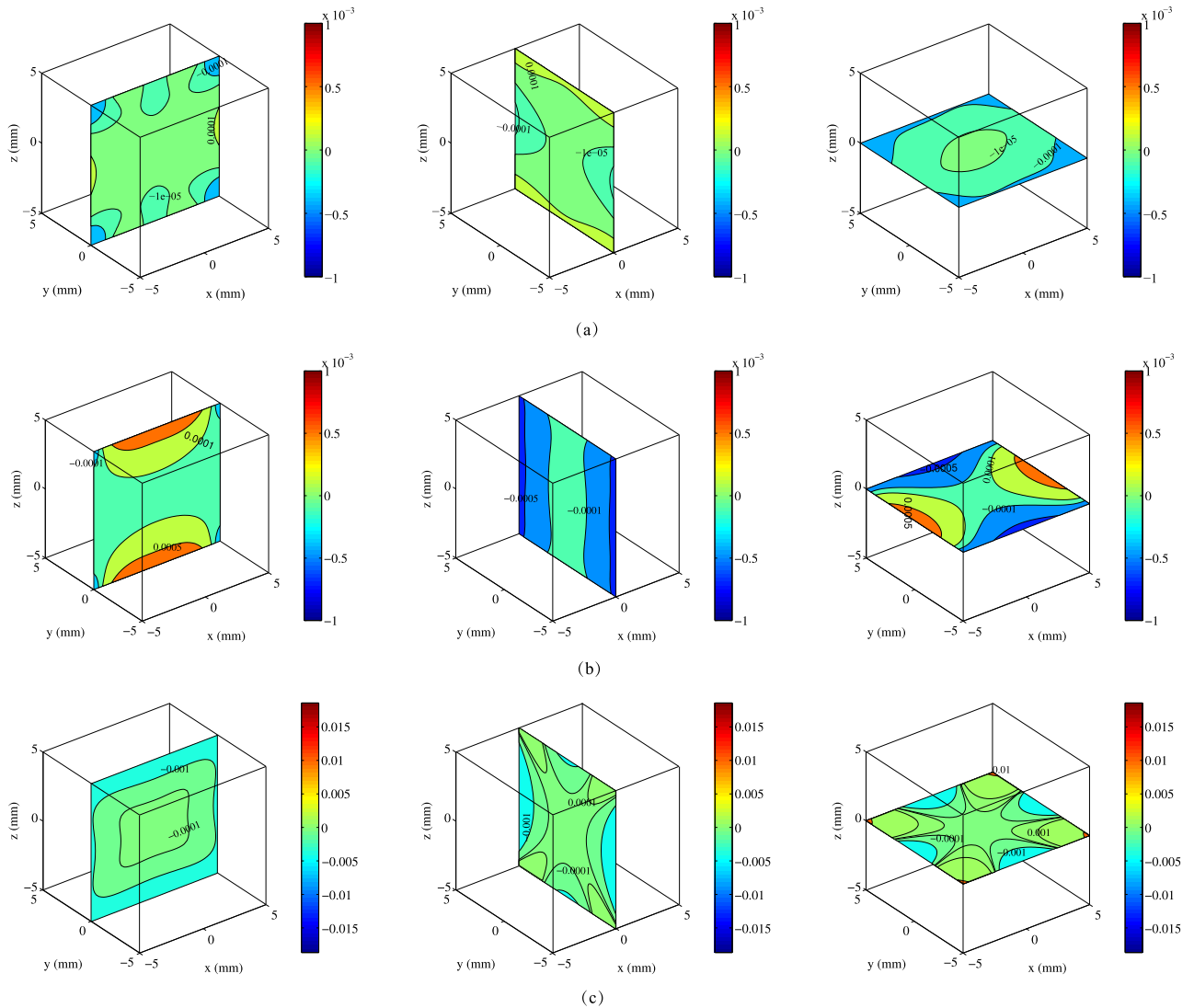
FIGURE 6. Magnetic field relative error distribution of three coils on three coordinate plans, showing the magnetic field distribution in the center of the coordinate plane with a side length of ±5 mm. (a) Designed coil 1; (b) designed coil 2; (c) nested saddle coil. The uniformity performances of coils designed by this method are obviously improved by about one order of magnitude than the nested saddle coil.

points along the *z*-axis from -86 mm to 89 mm, at 5 mm intervals. The second experiment was to calibrate the coil constant under different modulation currents along the *y*-axis.

A current generator named LDC 205C was used to produce AC modulation current as input to the coils. The AC current was sufficient to produce a stable magnetic field environment. The output signal of MAG-03 was demodulated by a lock-in amplifier named MFLI (Zurich Instruments). During the measurements of magnetic field along the axis position, AC currents with amplitudes of 125.93 mA, 162.25 mA and 216.15 mA all with frequency of 23 Hz, were applied to designed coil 1, designed coil 2 and nested saddle coil, respectively. The measurement results with uncertainties of each test coil are listed in Table 2. Considering that there is a gain attenuation in the output value of MAG-03 used in the range of AC frequency band, all the measured results were multiplied by the attenuation coefficient. Figure 8 shows a comparison between the simulation results
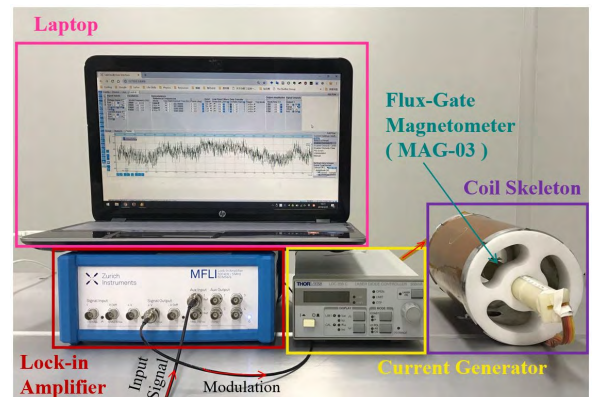
FIGURE 7. Actual magnetic field tests with a fluxgate magnetometer.

and the measurements. It can be seen from Fig.8 that the actual measurements are consistent with the simulation results. The magnitude of the magnetic field is approximately

J. Wang *et al.*: Improved Target-Field Method for the Design of Uniform Magnetic Field Coils in Miniature Atomic Sensors

IEEE *Access*

TABLE 2. Magnetic field measurement results.

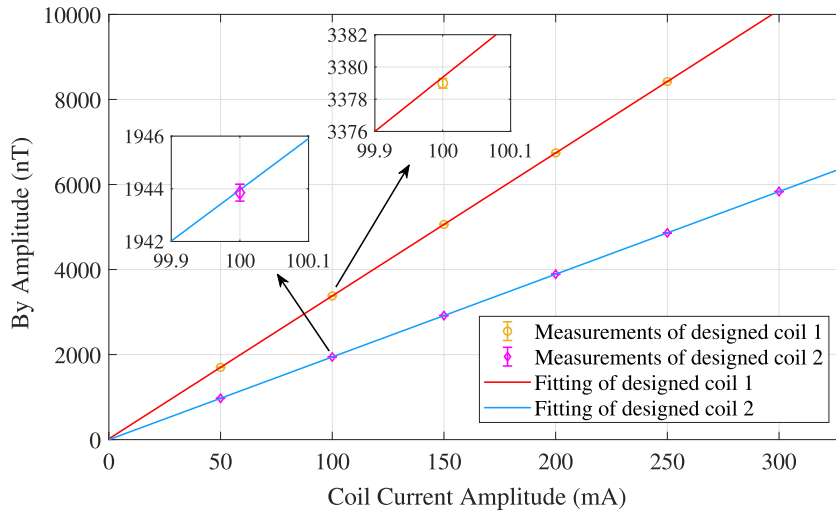| Points on the z-axis (mm)	Measurements of designed coil 1 (nT)	Error relative to the central magnetic field	Measurements of designed coil 2 (nT)	Error relative to the central magnetic field	Measurements of nested saddle coil (nT)	Error relative to the central magnetic field
−86	1399.430±0.314	53.6 %	675.718 ± 0.338	71.4 %	1784.611±0.419	33.9 %
−81	1598.284±0.251	47.0 %	902.962 ± 0.263	61.7 %	1880.791±0.245	30.3 %
−76	1803.297±0.322	40.2 %	1108.377±0.190	53.0 %	1985.332±0.429	26.4 %
−71	2019.375±0.220	33.0 %	1308.897±0.251	44.5 %	2092.579±0.238	22.5 %
−66	2268.463±0.205	24.8 %	1512.799±0.266	35.9 %	2198.712±0.222	18.5 %
−61	2501.128±0.231	17.1 %	1701.693±0.257	27.9 %	2299.299±0.242	14.8 %
−56	2652.230±0.229	12.1 %	1863.839±0.187	21.0 %	2389.213±0.185	11.5 %
−51	2807.971±0.171	6.9 %	2021.682±0.234	14.3 %	2491.336±0.211	7.7 %
−46	2904.545±0.189	3.7 %	2181.822±0.190	7.5 %	2550.363±0.310	5.5 %
−41	2965.411±0.306	1.7 %	2244.046±0.124	4.9 %	2616.696±0.382	3.0 %
−36	2995.582±0.226	0.7 %	2303.871±0.150	2.4 %	2653.041±0.280	1.7 %
−31	3001.816±0.203	0.5 %	2327.111±0.140	1.4 %	2677.749±0.188	0.8 %
−26	3007.850±0.290	0.26 %	2348.913±0.099	0.47 %	2691.416±0.355	0.28 %
−21	3015.091±0.209	0.022 %	2353.409±0.271	0.28 %	2698.68 ± 0.172	0.01 %
−16	3016.296±0.295	-0.018 %	2355.770±0.170	0.18 %	2699.501±0.265	-0.02 %
−11	3016.167±0.308	-0.014 %	2359.988±0.141	0	2698.861±0.352	0.004 %
−6	3016.274±0.537	-0.017 %	2359.849±0.148	0.006 %	2698.269±0.381	0.03 %
−1	3015.750±0.194	0	2359.468±0.160	0.02 %	2698.975±0.401	0
4	3015.859±0.280	-0.004 %	2359.710±0.162	0.01 %	2699.046±0.408	-0.003 %
9	3016.109±0.404	-0.02 %	2360.491±0.137	-0.02 %	2698.077±0.311	-0.004 %
14	3016.901±0.521	-0.04 %	2360.227±0.195	-0.01 %	2698.195±0.426	0.03 %
19	3016.579±0.208	-0.03 %	2359.154±0.349	0.03 %	2699.705±0.426	-0.03 %
24	3015.393±0.277	0.01 %	2354.826±0.379	0.3 %	2704.560±0.217	-0.2 %
29	3009.739±0.203	0.2 %	2339.158±0.635	0.9 %	2693.397±0.254	0.2 %
34	2993.356±0.391	0.7 %	2318.146±0.555	1.8 %	2664.856±0.356	1.3 %
39	2965.066±0.230	1.7 %	2293.660±0.195	2.8 %	2630.630±0.293	2.5 %
44	2898.802±0.392	3.9 %	2254.404±0.227	4.5 %	2582.799±0.387	4.3 %
49	2804.429±0.265	7.0 %	2169.646±0.138	8.1 %	2516.097±0.324	6.8 %
54	2665.069±0.207	11.6 %	2076.302±0.145	12.0 %	2420.609±0.198	10.3 %
59	2513.322±0.501	16.7 %	1906.750±0.151	19.2 %	2337.922±0.415	13.4 %
64	2373.959±0.390	21.3 %	1746.602±0.278	26.0 %	2241.465±0.267	17.0 %
69	2156.128±0.230	28.5 %	1513.607±0.262	35.9 %	2137.106 ± 245	20.8 %
74	1958.580±0.371	35.1 %	1254.582±0.295	46.8 %	2029.353±0.310	24.8 %
79	1773.939±0.264	41.2 %	1080.436±0.345	54.2 %	1923.476±0.149	28.7 %
84	1518.859±0.205	49.6 %	903.705 ± 0.406	61.7 %	1823.498±0.222	32.4 %
89	1299.064±0.273	56.9 %	673.524 ± 0.375	71.5 %	1735.257±0.235	35.7 %
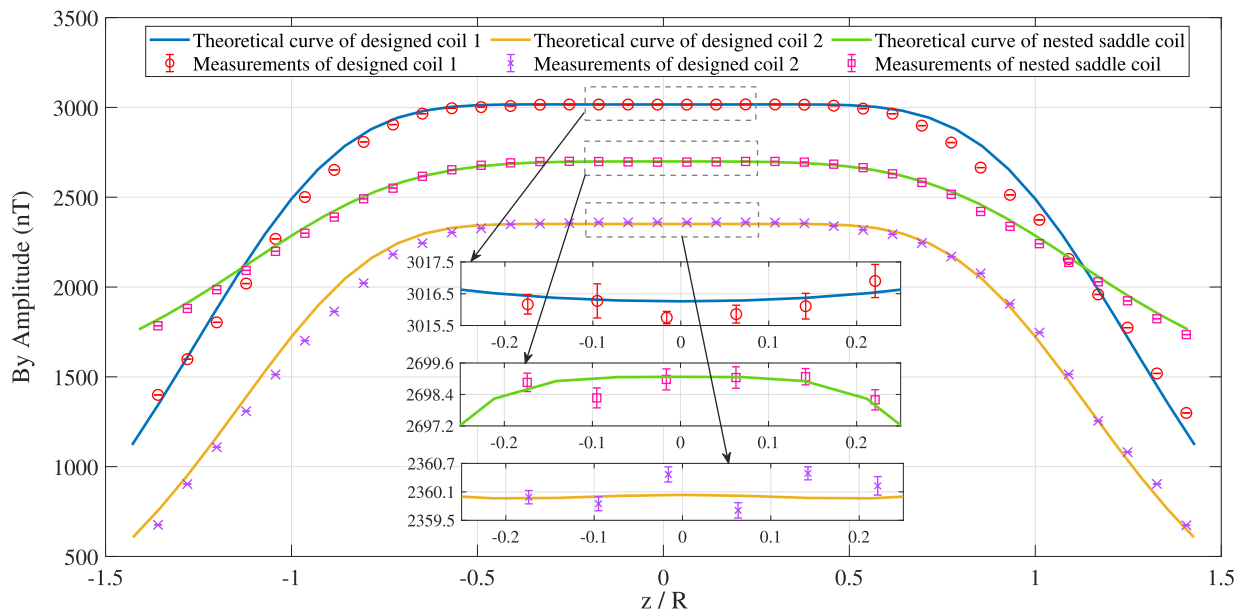
FIGURE 8. Measurements of magnetic field produced by the test coils along z-axis, with a distribution range of [−1.363 R, 1.41 R] (R = 63.1 mm). The red "o" and purple "x" markers show the measurements of the designed coil 1 and coil 2, respectively. The blue and the yellow solid lines indicate the theoretical value of the designed coil 1 and coil 2, respectively.

IEEE *Access*

J. Wang *et al.*: Improved Target-Field Method for the Design of Uniform Magnetic Field Coils in Miniature Atomic Sensors

FIGURE 9. Fitting of coil constants. The yellow 'o' and pink 'diamond' markers are the actual test data. The red and the blue solid lines are the fitting results of the designed coil 1 and coil 2.

TABLE 3. Magnetic field measurements at different coil currents along the $y-$axis.

Coil current amplitude (mA)	Magnetic field measurement of designed coil 1 (nT)	Magnetic field measurement of designed coil 2 (nT)
50	1699.173 ± 0.311	971.456 ± 0.318
100	3378.983 ± 0.297	1943.851 ± 0.320
150	5060.013 ± 0.301	2916.806 ± 0.322
200	6742.082 ± 0.324	3889.501 ± 0.312
250	8420.660 ± 0.285	4861.413 ± 0.263
300	———	5834.203 ± 0.277

the same in the TSV whose length is 0.5 times the radius of the coil.

In the calibration of coil constants, the experimental data with different coil current amplitudes are shown in Table 3 and Fig.9. The measured data were linearly fitted to obtain the coil constants 33.612 ± 0.020 nT/mA and 19.451 ± 0.004 nT/mA of the corresponding coils. The theoretical obtained coil constants of these two designed coils are 33.742 nT/mA and 19.482 nT/mA, respectively. There is remarkable consistency between theory and actual experiments.

V. CONCLUSION

In this paper, a new approach based on the TFM is proposed for the design of uniform magnetic field coil. The current density on the cylindrical coil surface is divided into two parts according to the symmetrical cross section of the coil and is expanded into Fourier series. A reserved gap for light-passing holes can be set by controlling the initial position of the upper and the lower parts of the current density in the coil center. The minimum curvature constraint is introduced as the penalty function of the current density and solved by Tikhonov regularization. The actual winding patterns are ultimately obtained by using the stream function method. The advantages of the proposed method are the high magnetic field uniformity and small space occupation of the coil.

Its characteristic lies in the flexibility of the control coil design process, whereas the distribution of the selected target field coordinates is not limited to the strategies adopted in this paper. TSV of other shapes can be further studied to improve the accuracy of the design. The performance of the proposed method is evaluated and compared with traditional nested saddle coil using both simulations and experimental measurements. This method can improve the uniformity performance by about one order of magnitude compared with the nested saddle coil. The comparative analysis validated that the proposed method is appropriate for not only miniature atomic sensors but also any situation where uniform magnetic field is required.
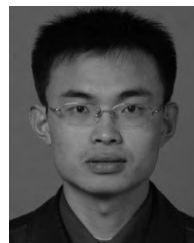
REFERENCES

[1] J. Kitching, S. Knappe, and E. A. Donley, "Atomic sensors—A review," *IEEE Sensors J.*, vol. 11, no. 9, pp. 1749–1758, Sep. 2011.

[2] V. Pasku, A. De Angelis, M. Dionigi, A. Moschitta, G. De Angelis, and P. Carbone, "Analysis of nonideal effects and performance in magnetic positioning systems," *IEEE Trans. Instrum. Meas.*, vol. 65, no. 12, pp. 2816–2827, Dec. 2016.

[3] B. E. Fischer, I. J. LaHaie, D. D. Arumugam, J. D. Griffin, D. D. Stancil, and D. S. Ricketts, "Three-dimensional position and orientation measurements using magneto-quasistatic fields and complex image theory," *IEEE Antennas Propag. Mag.*, vol. 56, no. 1, pp. 160–173, Feb. 2014.

[4] V. Pasku, A. D. Angelis, G. D. Angelis, D. D. Arumugam, M. Dionigi, and P. Carbone, "Magnetic field-based positioning systems," *IEEE Commun. Surveys Tuts.*, vol. 19, no. 3, pp. 2003–2017, 3rd Quart., 2017.

[5] C. Hu, S. Song, X. Wang, M. Q.-H. Meng, and B. Li, "A novel positioning and orientation system based on three-axis magnetic coils," *IEEE Trans. Magn.*, vol. 48, no. 7, pp. 2211–2219, Jul. 2012.

[6] S. Song, W. Qiao, B. Li, C. Hu, H. Ren, and M. Q.-H. Meng, "An efficient magnetic tracking method using uniaxial sensing coil," *IEEE Trans. Magn.*, vol. 50, no. 1, Jan. 2014, Art. no. 4003707.

[7] C. Hu, M. Li, S. Song, W. Yang, R. Zhang, and M. Q.-H. Meng, "A cubic 3-axis magnetic sensor array for wirelessly tracking magnet position and orientation," *IEEE Sensors J.*, vol. 10, no. 5, pp. 903–913, May 2010.

[8] G. De Angelis, A. Moschitta, A. De Angelis, and P. Carbone, "Validation and comparison of circular coils' inductive coupling models," *Measurement*, vol. 133, pp. 14–22, Feb. 2019.

J. Wang *et al.*: Improved Target-Field Method for the Design of Uniform Magnetic Field Coils in Miniature Atomic Sensors

IEEE *Access*

[9] S. K. Lee, K. L. Sauer, S. J. Seltzer, O. Alem, and M. V. Romalis, "Subfemtotesla radio-frequency atomic magnetometer for detection of nuclear quadrupole resonance," *Appl. Phys. Lett.*, vol. 89, Nov. 2006, Art. no. 214106.

[10] H. B. Dang, A. C. Maloof, and M. V. Romalis, "Ultrahigh sensitivity magnetic field and magnetization measurements with an atomic magnetometer," *Appl. Phys. Lett.*, vol. 97, no. 15, Oct. 2010, Art. no. 151110.

[11] J. Li, Q. Wei, B. Zhou, Z. Wang, J. Lu, Z. Hu, G. Liu, and J. Fang, "SERF atomic magnetometer–recent advances and applications: A review," *IEEE Sensors J.*, vol. 18, no. 20, pp. 8198–8206, Oct. 2018.

[12] L. Jiang, W. Quan, R. Li, W. Fan, F. Liu, J. Qin, S. Wan, and J. Fang, "A parametrically modulated dual-axis atomic spin gyroscope," *Phys. Rev. Lett.*, vol. 112, no. 5, 2018, Art. no. 054103.

[13] M. Larsen and D. Meyer, "Nuclear magnetic resonance gyro for inertial navigation," *Gyroscopy Navigat.*, vol. 5, no. 2, pp. 75–82, Apr. 2014.

[14] E. J. Eklund, "Microgyroscope based on spin-polarized nuclei," Ph.D. dissertation, Dept. Phys., Univ. California, Oakland, CA, USA, 2008.

[15] H. Zhang, S. Zou, and X. Chen, "Ingenious method for measuring the non-orthogonal angle of the saddle-shaped coils of an SERF atomic magnetometer system," *IEEE Trans. Magn.*, vol. 52, no. 10, Oct. 2016, Art. no. 4002906.

[16] W. Fan, G. Liu, R. Li, W. Quan, L. Jiang, and L. Duan, "A three-axis atomic magnetometer for temperature-dependence measurements of fields in a magnetically shielded environment," *Meas. Sci. Technol.*, vol. 28, no. 9, 2017, Art. no. 095007.

[17] S. Jeon, G. Jang, H. Choi, and S. Park, "Magnetic navigation system with gradient and uniform saddle coils for the wireless manipulation of micro-robots in human blood vessels," *IEEE Trans. Magn.*, vol. 46, no. 6, pp. 1943–1946, Jun. 2010.

[18] F. Bonetto, E. Anoardo, and M. Polello, "Saddle coils for uniform static magnetic field generation in NMR experiments," *Concepts Magn. Reson. B, Magn. Reson. Eng.*, vol. 29B, pp. 9–19, Feb. 2006.

[19] W. Wu, B. Zhou, G. Liu, L. Chen, J. Wang, and J. Fang, "Novel nested saddle coils used in miniature atomic sensors," *AIP Adv.*, vol. 8, Jul. 2018, Art. no. 075126.

[20] Y. J. Kim and I. Savukov, "Ultra-sensitive magnetic microscopy with an optically pumped magnetometer," *Sci. Rep.*, vol. 6, Apr. 2016, Art. no. 24773.

[21] I. Savukov, Y. J. Kim, V. Shah, and M. G. Boshier, "High-sensitivity operation of single-beam optically pumped magnetometer in a khz frequency range," *Meas. Sci. Technol.*, vol. 28, no. 3, 2017, Art. no. 035104.

[22] T. G. Walker and M. S. Larsen, "Spin-exchange-pumped NMR gyros," *Adv. At., Mol., Opt. Phys.*, vol. 65, pp. 373–401, Jan. 2016.

[23] J. Wang, B. Zhou, W. Wu, L. Chen, and J. Fang, "Uniform field coil design based on the target-field method in miniature atomic sensors," *IEEE Sensors J.*, vol. 19, no. 8, pp. 2895–2901, Apr. 2019.

[24] R. Turner, "A target field approach to optimal coil design," *J. Phys. D, Appl. Phys.*, vol. 19, pp. L147–L151, May 1986.

[25] R. Turner, "Minimum inductance coils," *J. Phys. E, Sci. Instrum.*, vol. 21, no. 10, pp. 948–952, 1988.

[26] W. Liu, D. Zu, X. Tang, and H. Guo, "Target-field method for MRI biplanar gradient coil design," *J. Phys. D, Appl. Phys.*, vol. 40, no. 15, pp. 4418–4424, 2007.

[27] W. Liu, F. Casanova, B. Blümich, and D. Zu, "An efficacious target-field approach to design shim coils for Halbach magnet of mobile NMR sensors," *Appl. Magn. Reson.*, vol. 42, pp. 101–112, Sep. 2012.

[28] P. T. While, L. K. Forbes, and S. Crozier, "3-D gradient coil design—Initial theoretical framework," *IEEE Trans. Biomed. Eng.*, vol. 56, no. 4, pp. 1169–1183, Apr. 2009.

[29] A. Phair, M. Brideson, and L. K. Forbes, "A cylindrical basis set for shim coil design in magnetic resonance imaging," *Concepts Magn. Reson. B, Magn. Reson. Eng.*, vol. 48, no. 3, 2018, Art. no. e21400. doi: 10.1002/cmr.b.21400.

[30] X. Li, D. Xie, and J. Wang, "A novel target field method for designing uniplanar self-shield gradient coils of fully open MRI device," *J. Electromagn. Waves Appl.*, vol. 21, pp. 1635–1644, Jan. 2007.

[31] Y. Wang, X. Xin, F. Liu, and S. Crozier, "Spiral gradient coil design for use in cylindrical MRI systems," *IEEE Trans. Biomed. Eng.*, vol. 65, no. 4, pp. 911–920, Apr. 2018.

[32] D. Tomasi, "Stream function optimization for gradient coil design," *Magn. Reson. Med.*, vol. 45, no. 3, pp. 505–512, 2001.

[33] L. K. Forbes and S. Crozier, "A novel target-field method for finite-length magnetic resonance shim coils: I. Zonal shims," *J. Phys. D, Appl. Phys.*, vol. 34, pp. 2001–3447, Dec. 2001.

[34] L. K. Forbes and S. Crozier, "A novel target-field method for finite-length magnetic resonance shim coils: II. Tesseral shims," *J. Phys. D, Appl. Phys.*, vol. 35, pp. 839–849, Apr. 2002.

[35] L. K. Forbes, M. A. Brideson, and S. Crozier, "A target-field method to design circular biplanar coils for asymmetric shim and gradient fields," *IEEE Trans. Magn.*, vol. 41, no. 6, pp. 2134–2144, Jun. 2005.

[36] L. K. Forbes and S. Crozier, "Novel target-field method for designing shielded biplanar shim and gradient coils," *IEEE Trans. Magn.*, vol. 40, no. 4, pp. 1929–1938, Jul. 2004.

[37] W. Xu, J. Zhang, and X. Li, "Designing shielded radio-frequency phased-array coils for magnetic resonance imaging," *Chin. Phys. B*, vol. 22, no. 1, 2013, Art. no. 010203.

[38] G. Hu, Z. Ni, and Q. Wang, "A novel target-field method using LASSO algorithm for shim and gradient coil design," *IEEE Trans. Appl. Supercond.*, vol. 22, no. 3, Jun. 2012, Art. no. 4900604.

JING WANG was born in Baoding, Hebei, China, in 1993. She received the B.S. degree from the School of Mechanical Engineering, Hebei University of Technology, Tianjin, China, in 2015. She is currently pursuing the Ph.D. degree with the School of Instrumentation Science and Opto-Electronics Engineering, Beihang University, Beijing, China. Her main research interests include uniform field coil design, inertial and magnetic measurements, atomic magnetometer, and MEG research.

BINQUAN ZHOU was born in Shanxi, China, in 1981. He received the Ph.D. degree in precision instrument and mechanics from Beihang University, in 2017, where he is currently an Assistant Professor with the School of Instrumentation Science and Optical Engineering. He has undertaken multiple national and ministerial research projects, including the National Natural Science Fund and the 863 of Ministry of Science and Technology. His research interests include atomic gyroscope, atomic magnetometer, and MEG research.

XU LIU was born in Shandong, China, in 1987. He received the B.S. degree from the Tianjin University of Science and Technology, Tianjin, China, in 2012, the Ph.D. degree from Beihang University, Beijing, China, in 2018, where he is currently a Postdoctoral Researcher with the Advanced Innovation Center for Big Data-Based Precision Medicine. His main research interests include inertial actuators mounted on the spacecraft, design of magnetically suspended high-speed motor, and hybrid magnetic bearing.

WENFENG WU received the B.S. degree from the Tianjin University of Science and Technology, Tianjin, China, in 2012, the M.S. degree from Shanghai University, Shanghai, China, in 2014. He is currently pursuing the Ph.D. degree with the School of Instrumentation Science and Opto-Electronics Engineering, Beihang University, Beijing. His main research interests include the design of magnetic shield systems, nuclear magnetic resonance gyroscope, and atomic magnetometer.

IEEE *Access*

J. Wang *et al.*: Improved Target-Field Method for the Design of Uniform Magnetic Field Coils in Miniature Atomic Sensors

LINLIN CHEN received the Ph.D. degree from Beihang University, in 2018. She is currently a Lecturer with the Department of Aerospace Science and Technology, Space Engineering University. Her research interests include atomic gyroscope, atomic magnetometer, and electronic-optical detection technology.

BANGCHENG HAN (M'14) was born in 1974. He received the B.S. degree in mechanotronics and the M.S. degree in mechanical design and theory from Jilin University, Changchun, China, in 2001, and the Ph.D. degree in mechanical design, manufacturing, and automation from the Changchun Institute of Optics, Fine Mechanics and Physics, Chinese Academy of Sciences, Changchun, in 2004. In 2004, he was a Postdoctoral Research Fellow with the School of Instrumentation and Opto-Electronics Engineering, Beihang University, Beijing, China. In 2006, he joined Beihang University, where he is currently a Professor with the School of Instrumentation and Opto-Electronics Engineering. He is also with the Beijing Engineering Research Center of High-Speed Magnetically Suspended Motor Technology and Application, Beihang University. He has authored/coauthored more than 50 journal and conference publications. His research interests include mechatronics, magnetic suspension technology, attitude control actuators of spacecraft, atomic magnetometers, atomic comagnetometers, and MEG research.

JIANCHENG FANG (M'11) was born in Shandong, China, in 1965. He received the B.S. degree in electrical engineering from the Shandong University of Technology, Jinan, China, in 1983, the M.S. degree in automotive engineering from Xi'an Jiao Tong University, Xi'an, China, in 1988, and the Ph.D. degree in mechanical engineering from Southeast University, Nanjing, China, in 1996. He is currently the Vice President of Beihang University, Beijing, China. He holds a special appointment professorship with the title of Cheung Kong Scholar, which was jointly established by the Ministry of Education of China and the Li Ka Shing Foundation. He has authored or coauthored over 150 papers and four books. His current research interests include the attitude control system technology of spacecraft, novel inertial instrument and equipment technology, inertial navigation, and SERF atomic magnetometer and co-magnetometer.

• • •